Engineering Fracture Mechanics 193 (2018) 162–171

Contents lists available at ScienceDirect

Engineering Fracture Mechanics

journal homepage: www.elsevier.com/locate/engfracmech

The effect of sweat on the performance of the interface between skin and flexible membrane

Weijie Xian[a], Yulan Liu[a,*], Biao Wang[b]

[a] School of Engineering, Sun Yat-sen University, Guangzhou 510275, PR China
[b] School of Physics, Sun Yat-sen University, Guangzhou 510275, PR China

ARTICLE INFO

Keywords:
Liquid bridge
Interfacial crack
Crack opening displacement
Stress intensity factor
Complex variable method

ABSTRACT

Upon realizing the importance of the sweat in controlling the performance of the interface crack between skin and flexible membrane, the effect of sweat on the crack opening under action of the far-field tensile stress is analysed in present paper. Application of the complex variable method and the principle of superposition gives the crack opening displacement and the stress intensity factors, which are functions of the surface tension, contact angle, location and size of the sweat. The location of sweat has important influence on the stress intensity factors, although it induces very little changes in the shape of the crack opening. Without or with the action of a small far-filed tensile stress, the sweat can induce the crack partial closure. With the increase of the far-field tensile stress, the crack opening displacement will be large enough to cause the disruption of the sweat, even induce the crack growth. So, the far-field tensile stress, which can split the sweat, is derived in present paper.

1. Introduction

In recent years, flexible electronics have attracted much attention due to their biocompatibility, high stretching ability and non-toxicity. Kim et al. [1] proposed an electronic system, incorporating the sensors, wireless power devices, electronic circuits and flexible membranes, matched to the epidermis. At present, the flexible electronics is mainly used in the medical area such as to measure electrical activity produced by brain, heart, skin and so on [2].

The measuring of physiological signals is crucial for medical diagnosis and therapeutics [3,4], so that it requires excellent physical contact between the flexible membrane and the epidermis. However, there may exit pores between flexible membrane and the epidermis in reality, and the sweat may appear in these pores to influence the contact between flexible membrane and epidermis. In modelling, we can regard the sweat as liquid bridges or capillary droplet. So, it's necessary to study the effect of the liquid bridge on the interface between skin and flexible membrane.

Recently, there have been many studies focusing on the local deformation of flexible membrane caused by a capillary droplet [6–8]. Yu and Zhao [9] gave the theoretical solution of the surface deformation of substrates with finite thickness induced by a sessile liquid droplet based on the Lester's assumptions by the virtue of Hankel transformation. Karpitschka et al. [10] analysed the stick-slip motion for viscoelastic capillary dynamics valid beyond droplets. Park et al. [11] proposed that the cusp of the ridge was bent with an asymmetric tip, which were determined by the surface stresses. Yang et al. [12] analysed the effect of a capillary bridge on the crack opening of a penny crack.

In summary, liquid bridges or liquid droplets play an important role in controlling the performance of the flexible membranes.

* Corresponding author.
E-mail address: stslyl@mail.sysu.edu.cn (Y. Liu).

https://doi.org/10.1016/j.engfracmech.2018.02.012
Received 12 August 2017; Received in revised form 8 February 2018; Accepted 11 February 2018
Available online 26 February 2018
0013-7944/ © 2018 Elsevier Ltd. All rights reserved.

Nomenclature

a	the crack length
b	the distance from the right bound of sweat bridge to the right tip of crack
c	the distance from the left bound of sweat bridge to the right tip of crack
$c-b$	the wetting area of sweat bridge
$(b+c)/2$	the distance between right tip and the centre of sweat bridge
E_j	Young's modulus (j = 1, 2)
G_j	shear modulus (j = 1, 2)
h	the initial height of sweat bridge
h_d	the equivalent height of sweat bridge
K	the overall stress intensity factors
$K1$	the stress intensity factors subjected to a pressure along part of the crack surface
$K2$	the stress intensity factors under the action of a far-field tensile stress
p	the capillary pressure of sweat bridge
$r_{L;R}$	the distance to the left or right tip of crack
S	the size of sweat bridge
$u_x;u_y$	displacement components
$\sigma_x;\sigma_y;\tau_{xy}$	stress components
γ	the surface tension of the sweat
δ	the thickness of the liquid-vapour interface
ε	the oscillation indexes
θ	polar coordinates based on the right tip of crack
$\theta_0;\theta_d$	the actual and equivalent contact angle of sweat bridge
ν_j	Poisson's ratio (j = 1,2)
σ_0	far-field tensile stress
σ_m	the far-field tensile stress which ruptures the sweat bridge
χ	the stress over the liquid-vapour interface
$\Delta1$	the crack opening under the action of a pressure along part of the crack surface
$\Delta2$	the crack opening under the action of a far-field tensile stress
$\Phi_j(z);\Psi_j(z)$	Goursat functions (j = 1,2)
$\overline{X}$	complex conjugate of parameter X
$\widetilde{X}$	dimensionless form of parameter X

And in this study, we investigate the effect of a liquid bridge on the crack opening and the stress intensity factor of an interface crack between skin and flexible membrane (such as silicone). At first, we theoretically analyse the solutions of an interface crack subjected to a uniform pressure along part of the crack surface by using the complex variable method. And then the crack opening displacement and the stress intensity factor of an interface crack under concurrent action of sweat bridge and far-field tensile stress are calculated by using the principle of superposition. Finally, numerical calculations have been carried out to show the influences of the sweat's location and size on the crack opening displacement and the stress intensity factors.

2. Formulation of the problem

Yu et al. [9] found that there is a saturation membrane thickness of millimetre scale. If the thickness is larger than the saturation value, the membrane can be regarded as a semi-infinite solid. Consider a stationary interface crack with a stationary liquid bridge in an infinite space shown as in Fig. 1.

By using the complex variable method [13,14], the solutions of the interface crack shown as in Fig. 1 depend on the four unknown complex functions $\Phi_j(z)$ and $\Psi_j(z)$, j = 1,2, of the complex variable $z = x + iy = re^{i\theta}$. The basic equations are

$$\begin{cases} (\sigma_x)_j + (\sigma_y)_j = 4\mathrm{Re}[\Phi_j(z)] \\ (\sigma_x)_j - (\sigma_y)_j + 2i(\tau_{xy})_j = 2[\overline{z}\Phi'_j(z) + \Psi_j(z)] \\ 2G_j(u_x + iu_y)_j = \eta_j \int \Phi_j(z)dz - z\overline{\Phi}_j(\overline{z}) - \int \overline{\Psi}_j(\overline{z})d\overline{z} \end{cases} \tag{1}$$

where η_j is $3-4\nu_j$ for plane strain and $(3-4\nu_j)/(1+\nu_j)$ for plane stress, G_j is shear modulus.

Before solving this problem, the oscillation index ε is defined as

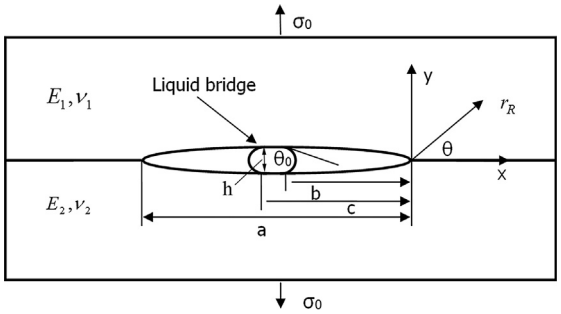

Fig. 1. Schematic of an interface crack with a liquid bridge in an infinite space.

$$\varepsilon = \frac{1}{2\pi}\ln\left[\left(\frac{\eta_1}{G_1}+\frac{1}{G_2}\right)\Big/\left(\frac{\eta_2}{G_2}+\frac{1}{G_1}\right)\right] \tag{2}$$

According to Rice [13,16], stress intensity factors in general may be considered as the strength of the stress singularities at crack tips and can be expressed as

$$\begin{Bmatrix} K_R \\ K_L \end{Bmatrix} = (k_1 + ik_2)\sqrt{\pi}\cosh(\pi\varepsilon) = 2\sqrt{2\pi}\cosh(\pi\varepsilon)\begin{Bmatrix} e^{\pi\varepsilon}\overline{Lim_{z\to 0} z^{(0.5+i\varepsilon)}\Phi_1(z)} \\ e^{-\pi\varepsilon}\overline{Lim_{z\to -a}(-z-a)^{(0.5+i\varepsilon)}\Phi_1(z)} \end{Bmatrix} \tag{3}$$

where $\overline{X}$ means the complex conjugate of parameter X.

The boundary and continuity conditions for the interface crack in Fig. 1 are

$$\sigma_y(x,0^+) - i\tau_{xy}(x,0^+) = \sigma_y(x,0^-) - i\tau_{xy}(x,0^-) \quad x > 0 \wedge x < -a \tag{4}$$

$$u_x(x,0^+) + iu_y(x,0^+) = u_x(x,0^-) + iu_y(x,0^-) \quad x > 0 \wedge x < -a \tag{5}$$

$$\tau_{xy}(x,0^+) = \tau_{xy}(x,0^-) = 0 \quad -a < x < 0 \tag{6}$$

$$\sigma_y(x,\pm\infty) = \sigma_0 \quad -\infty < x < +\infty \tag{7}$$

Lester [15] supposed the liquid-vapour interface of the liquid droplet had a thickness of δ, and the surface tension acted uniformly in the zone of this thickness, just like Fig. 2.

Similarly, the capillary pressure p and the normal stress over the liquid-vapour interface χ of the liquid bridge [12] shown in Fig. 1 can be calculated as

$$p = \frac{2\gamma\cos\theta_0}{h}; \chi = \frac{\gamma\sin\theta_0}{\delta} \tag{8}$$

And the normal stress on the crack surface can be obtained as

$$\sigma_y(r_R,\pm\pi) = \begin{cases} p & b \leqslant r_R \leqslant c \\ \chi & b-\delta \leqslant r_R < b \wedge c < r_R \leqslant c+\delta \\ 0 & \text{else} \end{cases} \tag{9}$$

Before solving this problem, the following dimensionless parameters are introduced:

$$\begin{cases} \widetilde{r}_R = \frac{r_R}{a}; \widetilde{b} = \frac{b}{a}; \widetilde{c} = \frac{c}{a}; \widetilde{\delta} = \frac{\delta}{a}; \widetilde{h} = \frac{h}{a}; \widetilde{h}_d = \frac{h_d}{a}; \widetilde{S} = \frac{S}{a^2} \\ \widetilde{u}_x = \frac{u_x}{a}; \widetilde{u}_y = \frac{u_y}{a}; \widetilde{\Delta} = \frac{\Delta}{a}; \widetilde{\Delta}1 = \frac{\Delta 1}{a}; \widetilde{\Delta}2 = \frac{\Delta 2}{a} \end{cases} \tag{10}$$

Using the principle of superposition, the interfacial crack problem with the boundary conditions of Eq. (6)–(9) can be transformed into the following three sub-problems [12].

Sub-problem I and II:

The normal stresses on the crack surface are

$$\sigma_y^1(\widetilde{r}_R,\pm\pi) = \begin{cases} \chi & \widetilde{b}-\widetilde{\delta} \leqslant \widetilde{r}_R \leqslant \widetilde{c}+\widetilde{\delta} \\ 0 & 0 < \widetilde{r}_R < \widetilde{b}-\widetilde{\delta} \wedge \widetilde{c}+\widetilde{\delta} < \widetilde{r}_R < 1 \end{cases} \tag{11}$$

$$\sigma_y^2(\widetilde{r}_R,\pm\pi) = \begin{cases} p-\chi & \widetilde{b} \leqslant \widetilde{r}_R \leqslant \widetilde{c} \\ 0 & 0 < \widetilde{r}_R < \widetilde{b} \wedge \widetilde{c} < \widetilde{r}_R < 1 \end{cases} \tag{12}$$

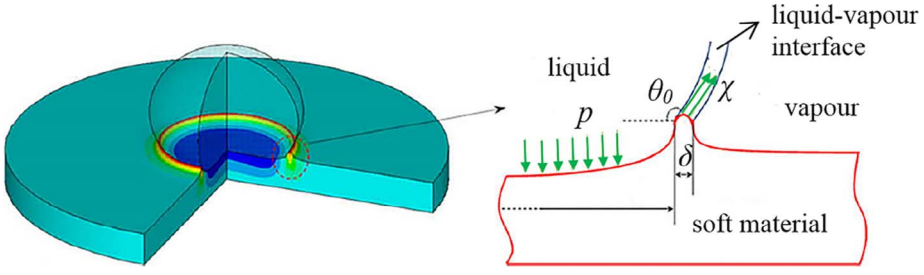

Fig. 2. Sketch of deformation and stress analysis of soft material induced by a water droplet [9].

Sub-problem III:

The normal stress on the crack surface is

$$\sigma_y^3(\tilde{r}_R,\pm\pi) = -\sigma_0 \quad 0 < \tilde{r}_R < 1 \tag{13}$$

which represents the equivalent pressure applied on the crack surface due to the far-field tensile stress.

3. The crack opening displacement and stress intensity factor

3.1. Preliminary solution based on sub-problem I and II

Application of the method of Rice [13] to Eq. (1)–(3), by virtue of the boundary conditions of (4)–(6), gives the four complex functions mentioned in Eq. (1) as

$$\begin{Bmatrix}\Phi_1(z)\\ \Phi_2(z)\end{Bmatrix} = \begin{Bmatrix}1\\ e^{2\pi\varepsilon}\end{Bmatrix} z^{-0.5-i\varepsilon}(z+a)^{-0.5+i\varepsilon} g(z) \tag{14}$$

$$\begin{Bmatrix}\Psi_1(z)\\ \Psi_2(z)\end{Bmatrix} = \begin{Bmatrix}e^{2\pi\varepsilon}\\ 1\end{Bmatrix} z^{-0.5+i\varepsilon}(z+a)^{-0.5-i\varepsilon}\overline{g}(z) - \begin{Bmatrix}1\\ e^{2\pi\varepsilon}\end{Bmatrix} z^{-0.5-i\varepsilon}(z+a)^{-0.5+i\varepsilon}\left[\frac{a(0.5-i\varepsilon)}{z+a} g(z) + z g'(z)\right] \tag{15}$$

Then the function $g(z)$ is given as

$$g(z) = \frac{pa}{2\pi e^{\pi\varepsilon}} \sum_{n=-\infty}^{+\infty} \begin{Bmatrix}C1_n(\tilde{b},\tilde{c})\\ C2_n(\tilde{b},\tilde{c})\\ C3_n(\tilde{b},\tilde{c})\end{Bmatrix} \tilde{z}^n \begin{Bmatrix}\tilde{r}_R < \tilde{b}\\ \tilde{b} \leqslant \tilde{r}_R \leqslant \tilde{c}\\ \tilde{r}_R > \tilde{c}\end{Bmatrix} \tag{16}$$

And the crack opening displacement in Fig. 3 is obtained as

$$\tilde{\Delta}1(p,\tilde{b},\tilde{c},\tilde{r}_R) = (\tilde{u}_x + i\tilde{u}_y)_{\theta=+\pi} - (\tilde{u}_x + i\tilde{u}_y)_{\theta=-\pi} = \frac{pi}{4\pi}\left(\frac{\eta_1+1}{G_1} + \frac{\eta_2+1}{G_2}\right) \sum_{-\infty}^{+\infty} \begin{Bmatrix}D_1(\tilde{b},\tilde{c})\\ D_2(\tilde{b},\tilde{c})\\ D_3(\tilde{b},\tilde{c})\end{Bmatrix} \tilde{r}_R^{n+0.5-i\varepsilon}(-1)^n \begin{Bmatrix}\tilde{r}_R < \tilde{b}\\ \tilde{b} < \tilde{r}_R < \tilde{c}\\ \tilde{r}_R > \tilde{c}\end{Bmatrix} \tag{17}$$

And the stress intensity factors under the action of pressure p along part of the crack face, $K1_R$ and $K1_L$, are obtained as

$$\begin{Bmatrix}K1_R(p,\tilde{b},\tilde{c})\\ K1_L(p,\tilde{b},\tilde{c})\end{Bmatrix} = pa^{0.5-i\varepsilon}\sqrt{\frac{2}{\pi}}\cosh(\pi\varepsilon) \begin{Bmatrix}\overline{C1}_0(\tilde{b},\tilde{c})\\ \sum_{-\infty}^{+\infty} \overline{C3}_n(\tilde{b},\tilde{c})(-1)^n\end{Bmatrix} \tag{18}$$

where the subscript R and L denote to the right and left tip of crack, respectively.

The above unknown parameters are given by

$$\begin{Bmatrix}A_0\\ B_0\end{Bmatrix} = \begin{Bmatrix}1\\ 1\end{Bmatrix}\begin{Bmatrix}A_n\\ B_n\end{Bmatrix} = \begin{Bmatrix}\prod_{j=1}^{n}(1.5-j-i\varepsilon)\\ (-1)^n\prod_{j=1}^{n}(j-0.5-i\varepsilon)\end{Bmatrix} \Big/ \; n! \quad 1 \leqslant n \leqslant m \tag{19}$$

where m is the order of Taylor series expansion, and the larger m is, the more accurate the solution is.

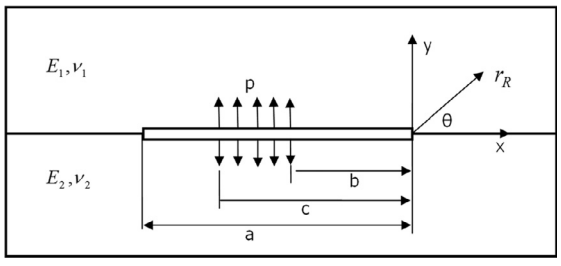

Fig. 3. An interface crack subjected to pressure p along part of the crack surface.

$$k1 = k + 0.5 + i\varepsilon - n$$
$$\begin{Bmatrix} C1_n(\widetilde{b},\widetilde{c}) \\ C2_n(\widetilde{b},\widetilde{c}) \\ C3_n(\widetilde{b},\widetilde{c}) \end{Bmatrix} = \sum_{k=0}^{m} \frac{A_k}{k1} \begin{Bmatrix} \widetilde{c}^{k1} - \widetilde{b}^{k1} \begin{Bmatrix} \widetilde{b}^{k1} \\ \widetilde{c}^{k1} \end{Bmatrix} \\ \widetilde{c}^{k1} - \widetilde{b}^{k1} \end{Bmatrix} \begin{Bmatrix} 0 \leqslant n \leqslant m \\ \begin{Bmatrix} -m-1 \leqslant n \leqslant -1 \\ 0 \leqslant n \leqslant m \end{Bmatrix} \\ -m-1 \leqslant n \leqslant -1 \end{Bmatrix} \tag{20}$$

where $C1_n$, $C2_n$ and $C3_n$ are the parameters to describe the stress field and the stress intensity factors.

$$\begin{Bmatrix} D1_n(\widetilde{b},\widetilde{c}) \\ D2_n(\widetilde{b},\widetilde{c}) \\ D3_n(\widetilde{b},\widetilde{c}) \end{Bmatrix} = \frac{\sum_{l=0}^{m} B_{n-l}}{n + 0.5 + i\varepsilon} \begin{Bmatrix} C1_l \\ C2_l \\ C3_l \end{Bmatrix} \begin{Bmatrix} 0 \leqslant n \leqslant 2m \\ -m-1 \leqslant n \leqslant 2m \\ -m-1 \leqslant n \leqslant m-1 \end{Bmatrix} \tag{21}$$

where $D1_n$, $D2_n$ and $D3_n$ are the parameters to describe the displacement field.

3.2. The accuracy of the preliminary solution

When $\widetilde{b} = 0$ and $\widetilde{c} = 1$, the solutions of the interface crack shown as in Fig. 3 reduce to those of an interface crack with uniform stress on the crack surface shown in Fig. 4c.

In Fig. 4b, the stress intensity factor of crack-free body is zero and the vertical displacement is zero at the interface due to symmetry. Therefore, the stress intensity factors and crack opening displacement of the interface crack shown in Fig. 4c are equivalent to that of Fig. 4a. So, crack opening displacement [16,17] of the interface crack shown in Fig. 4c can be expressed as

$$\widetilde{\Delta}2(\sigma_0,\widetilde{r}_R) = \frac{\sigma_0 i}{4\cosh(\pi\varepsilon)} \left(\frac{\eta_1 + 1}{G_1} + \frac{\eta_2 + 1}{G_2} \right) \begin{Bmatrix} \widetilde{r}_R^{0.5-i\varepsilon}(1-\widetilde{r}_R)^{0.5+i\varepsilon} \\ (1-\widetilde{r}_R)^{0.5-i\varepsilon}\widetilde{r}_R^{0.5+i\varepsilon} \end{Bmatrix} \begin{matrix} 0 \leqslant \widetilde{r}_R \leqslant 0.5 \\ 0.5 < \widetilde{r}_R \leqslant 1 \end{matrix} \tag{22}$$

and the stress intensity factor under the action of a far-field tensile stress [16,17] as

$$K2(\sigma_0) = \sigma_0 a^{0.5-i\varepsilon} \sqrt{\frac{\pi}{2}} (1 + 2\varepsilon i) \tag{23}$$

To estimate the accuracy of present analytic solutions, comparison is made with the solutions of the crack opening displacement and stress intensity factors provide by Rice et al., i.e. comparing Eq. (17), (18) with Eq. (22), (23) respectively. The following parameters are used in the calculation: $\widetilde{b} = 0$, $\widetilde{c} = 1$, $E_1 = 65$ kPa, $\nu_1 = 0.48$, $E_2 = 130$ kPa, $\nu_2 = 0.43$ and $\sigma_0 = 15$ kPa.

Fig. 5 and Table 1 depict the crack opening displacement and the stress intensity factors obtained by two different methods. Clearly, very accurate results are obtained by present analytic solutions.

3.3. The solutions of the interface crack problem shown in Fig. 1

By applying the principle of superposition to Eq. (17) and (18) and (22), (23), by the virtue of (11)–(13), the crack opening displacement of the interface crack shown in Fig. 1 is obtained as

$$\widetilde{\Delta}(\widetilde{r}_R) = \widetilde{\Delta}1\left(-\frac{\gamma\sin\theta_0}{\widetilde{\delta}a}, \widetilde{b} - \widetilde{\delta}, \widetilde{c} + \widetilde{\delta}, \widetilde{r}_R \right) + \widetilde{\Delta}1\left(-\frac{2\gamma\cos\theta_0}{\widetilde{h}a} + \frac{\gamma\sin\theta_0}{\widetilde{\delta}a}, \widetilde{b}, \widetilde{c}, \widetilde{r}_R \right) + \widetilde{\Delta}2(\sigma_0,\widetilde{r}_R) \tag{24}$$

and the stress intensity factors can be expressed as

$$K_{L;R} = K1_{L;R}\left(-\frac{\gamma\sin\theta_0}{\widetilde{\delta}a}, \widetilde{b} - \widetilde{\delta}, \widetilde{c} + \widetilde{\delta} \right) + K1_{L;R}\left(-\frac{2\gamma\cos\theta_0}{\widetilde{h}a} + \frac{\gamma\sin\theta_0}{\widetilde{\delta}a}, \widetilde{b}, \widetilde{c} \right) + K2(\sigma_0) \tag{25}$$

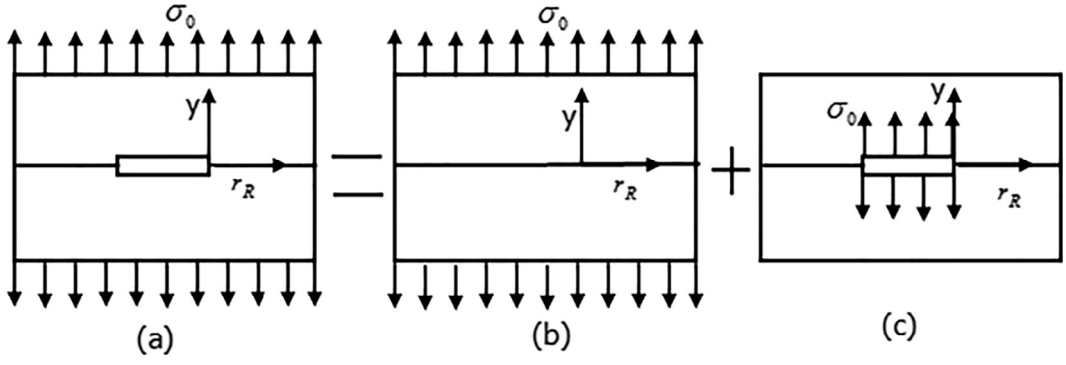

Fig. 4. Schematic of the principle of superposition.

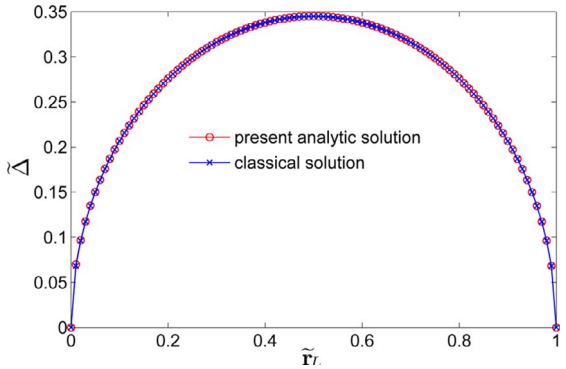

Fig. 5. The crack opening displacement obtained by two solutions.

Table 1
Stress intensity factors obtained by two solutions ($K = K_I + K_{II}\, I$ and dimensionless parameters $K^* = K/\sigma_0/(a)^{0.5-ic}$).

Classical solution [16,17]		Present analytic solution	
$K2_I^*$	$K2_{II}^*$	$K1_I^*$	$K1_{II}^*$
1.25331	0.06263	1.25339	0.06261

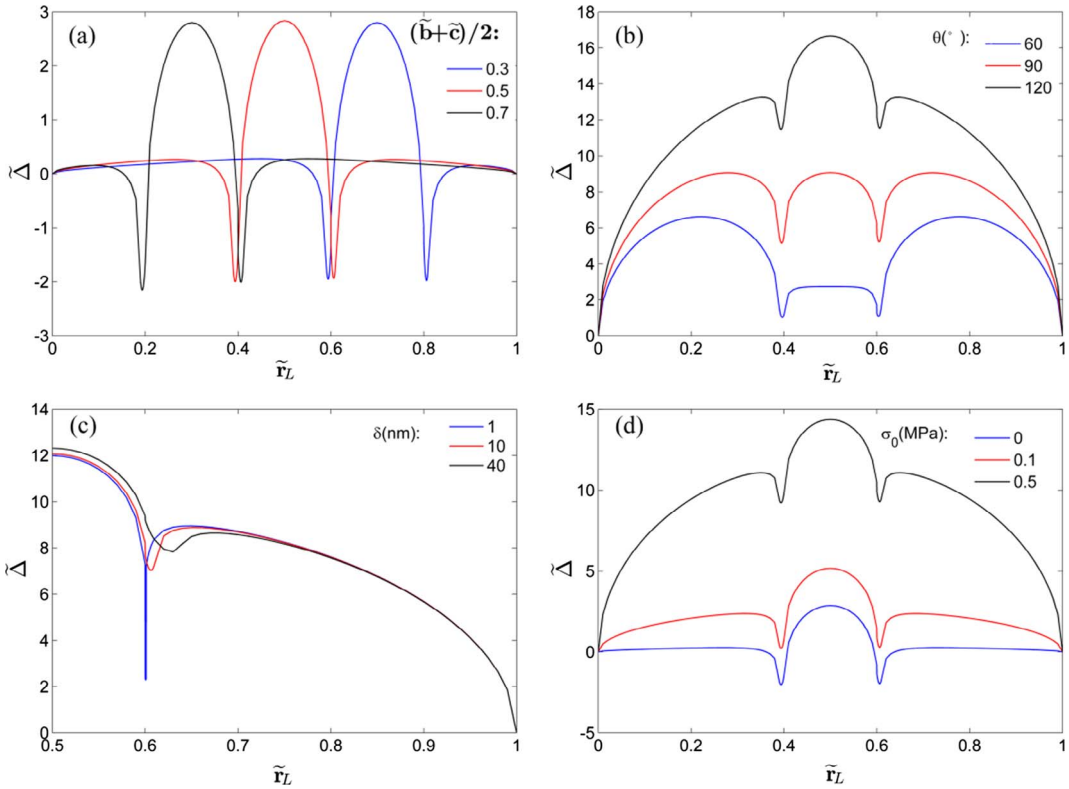

Fig. 6. The crack opening displacement under the action of different variables: (a) the location of sweat; (b) the contact angle; (c) the thickness of the liquid-vapour interface; (d) the far-field tensile stress.

where $\widetilde{\Delta}1$ and $\widetilde{\Delta}2$ are from Eq. (17) and (22) respectively, $K1_{L;R}$ are from Eq. (18), $K2$ is from Eq. (23).

4. Numerical results and discussion

4.1. Univariate analysis

Numerical results are obtained to demonstrate the effect of the sweat bridge on the interface crack opening displacement and the stress intensity factors. Consider an interface crack between the flexible membrane (such as silicone) and skin, subjected to the action of a sweat bridge. The Young's modulus of silicone E_1 and skin E_2 are 65 kPa and 130 kPa [5], respectively. The Poisson ratio of silicone ν_1 and skin ν_2 are 0.48 and 0.43, respectively. The surface tension of water γ is 72 $mN*m^{-1}$. The initial height of sweat h is 0.1 μm. Yu and Zhao [9,12] used 1, 10, 40 nm for δ in their analysis. The unit of p or χ, which is calculated in Eq. (8) by using above parameters, is "MPa", so that the unit of the remote tensile stress σ_0 is given as "MPa" in the following calculation.

Fig. 6 shows the effect of different variables on the crack opening displacement by using the following common parameters: $a = 1$ μm [12], $c - b = 0.2a$, $\delta = 10$ nm. The different variables in each figure are as follow: (a) $\sigma_0 = 0$ MPa, $\theta_0 = 120^\circ$ and supposing b to be $0.2a$, $0.4a$ and $0.6a$, respectively; (b) $\sigma_0 = 0.6$ MPa, $b = 0.2a$ and supposing θ_0 to be 60°, 90° and 120°, respectively; (c) $\sigma_0 = 0.4$ MPa, $\theta_0 = 120^\circ$ and supposing δ to be 1,10 and 40 nm, respectively; (d) $\delta = 10$ nm, $\theta_0 = 120^\circ$ and supposing σ_0 to be 0, 0.1 and 0.5 MPa in the calculation.

We find that the crack opening shown in Fig. 6 all have ridges at the boundary of the sweat bridge. This phenomenon is due to the normal stress over the liquid-vapour interface. In Eq. (8), δ is less than h, so that χ is larger than p. Larger stress will lead to larger deformation on the crack surface, so the deformation over the liquid-vapour interface is larger and the ridge exits at the boundary of sweat bridge.

As shown in Fig. 6a and Table 2, the maximum crack opening displacement increases slightly when the sweat is closer to the centre of crack. And Table 2 shows that the stress intensity factor decreases when sweat is apart from the crack tip. So that we can consider that the location of sweat is an important variable on the crack growth, although it induces the shape of crack opening to change slightly.

From Fig. 6b and Table 2, it is evident that the larger the contact angle is, the larger the crack opening displacement will be and the stress intensity factor manifests the same trend. However, the crack opening displacement along the contact line is less than that apart from the sweat bridge when the contact angle is less than 90°. This result is due to the fact that the overall capillary force is tensile on the crack surface when the contact angle is less than 90°, according to Eq. (8).

Fig. 6c shows us that the crack opening displacement decreases and the wetting ridges become smoother with the increase of the capillary layer's breadth δ. Such behaviour is induced by the vertical component of the surface tensions over the wetting ridges according to Eqs. (8) and (9). The larger the δ is, the smaller χ will be. Smaller stress will lead to smaller deformation on the crack surface. In addition, Table 2 shows that the capillary layer's breadth δ induces the change of the stress intensity factor slightly.

From Fig. 6d, we can find that without the action of a far-field tensile stress or with the action of a small far-field tensile stress, there may exist overlap between two crack surfaces. Such phenomenon is due to the vertical component of the surface tensions over the wetting ridges. And the size of sweat bridge also influences the size of crack closure.

4.2. Analysis in consideration of the actual crack shape

From Eq. (24), we know that the calculation of the crack opening displacement depends on the initial height of sweat bridge h, however the shape of sweat bridge is related to the crack opening displacement in reality, just like Fig. 7a. So, it is not reasonable to give the initial height of sweat bridge directly to calculate the crack opening displacement, which may lead to the unreasonable situation that the crack opening displacement far outweigh the initial height of sweat, just like Fig. 6. To solve the above problem, we can consider that the size of actual sweat is the same to that of the equivalent crack, i.e. $(S_1 + S_2 + S_3)_{\text{actual}} = (S_1 + S_2 + S_3)_{\text{equivalent}}$.

$$\begin{cases} (S_1)_{\text{actual}} = \frac{\Delta_y^2(b)}{4}\left(\frac{\theta_0 - \pi/2}{\cos^2\theta_0} - \tan\theta_0\right) \\ (S_2)_{\text{actual}} \approx \frac{1}{4}\left[\Delta_y(c) + 2\Delta_y\left(\frac{b+c}{2}\right) + \Delta_y(b)\right](c-b) \\ (S_3)_{\text{actual}} = \frac{\Delta_y^2(c)}{4}\left(\frac{\theta_0 - \pi/2}{\cos^2\theta_0} - \tan\theta_0\right) \end{cases} \tag{26}$$

Table 2
The maximum crack opening in Fig. 6a and the stress intensity factors to the right tip in Fig. 6a–c. ($K_R = K_{RI} + K_{RII}$ I).

Fig. 6-a				Fig. 6-b			Fig. 6-c		
$\widetilde{r}_R$	$\widetilde{\Delta}_{\max}$	K_{RI} (Pa $m^{0.5-ie}$)	K_{RII}	θ_0 (°)	K_{RI}	K_{RII}	δ (nm)	K_{RI}	K_{RII}
0.3	2.80	16.30	5.85	60	489.77	215.72	1	476.63	197.87
0.5	2.84	13.11	4.75	90	584.08	249.69	10	476.45	197.79
0.7	2.80	9.20	3.53	120	708.09	294.39	40	475.76	197.46

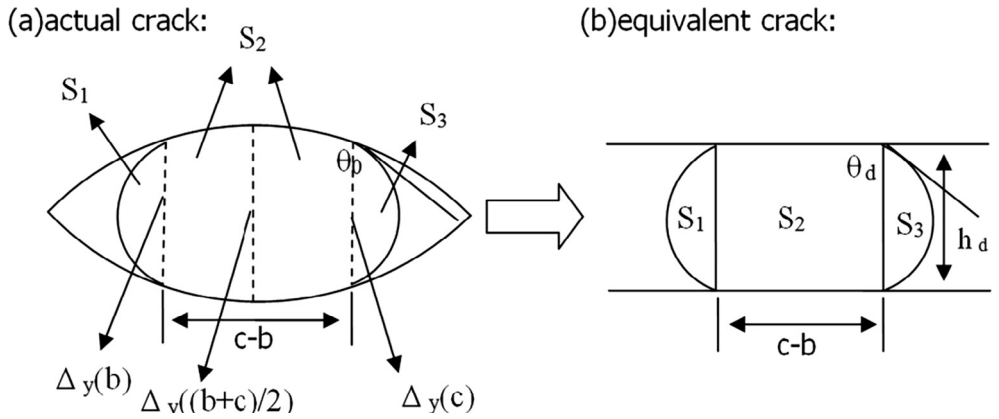

Fig. 7. Sketch of actual crack and equivalent crack (Δ_y is the vertical component of crack opening).

$$\begin{cases} (S_1)_{\text{equivalent}} = \frac{h_d^2}{4}\left(\frac{\theta_d - \pi/2}{\cos^2\theta_d} - \tan\theta_d\right) \\ (S_2)_{\text{equivalent}} = (c-b)h_d \\ (S_3)_{\text{equivalent}} = \frac{h_d^2}{4}\left(\frac{\theta_d - \pi/2}{\cos^2\theta_d} - \tan\theta_d\right) \end{cases} \tag{27}$$

where $\Delta_y(r_R)$ is the imaginary part of $\Delta(r_R)$, i.e. $\Delta_y(r_R) = \text{Im}[\Delta(r_R)]$.

In consideration of the following three points: the unknown relation between θ_0 and θ_d, the complexity of $\Delta_y^2(b)$ and the fact that the value of h_d is between $\Delta_y(b)$ and $\Delta_y[(b+c)/2]$, we may assume that the sizes of part S1 and S2 are approximately equal, i.e. $(S_1)_{\text{actual}} \approx (S_1)_{\text{equivalent}}$ and $(S_3)_{\text{actual}} \approx (S_3)_{\text{equivalent}}$, respectively. So, the relationship between h_d and $\Delta_y(r_R)$ is

$$(S_2)_{\text{actual}} = (S_2)_{\text{equivalent}}$$

$$\widetilde{h}_d = \frac{1}{4}\left[\widetilde{\Delta}_y(\widetilde{c}) + 2\widetilde{\Delta}_y\left(\frac{\widetilde{b}+\widetilde{c}}{2}\right) + \widetilde{\Delta}_y(\widetilde{b})\right] \tag{28}$$

Substituting Eq. (24) into Eq. (28), we have

$$4\widetilde{h}_d^2 - \widetilde{h}_d[I_{11} + \sigma_0 I_{12}] + I_2 = 0 \tag{29}$$

By solving Eq. (29), the equivalent height of sweat bridge can be expressed as

$$\widetilde{h}_d = \frac{[I_{11} + \sigma_0 I_{12}] + \sqrt{[I_{11} + \sigma_0 I_{12}]^2 - 16I_2}}{8} \tag{30}$$

where

$$\begin{Bmatrix} E1(\widetilde{r}_R) \\ E2(\widetilde{r}_R) \\ F(\widetilde{r}_R) \end{Bmatrix} = \begin{Bmatrix} \widetilde{\Delta}1(p,\widetilde{b}-\widetilde{\delta},\widetilde{c}+\widetilde{\delta},\widetilde{r}_R)/p \\ \widetilde{\Delta}1(p,\widetilde{b},\widetilde{c},\widetilde{r}_R)/p \\ \widetilde{\Delta}2(\sigma_0,\widetilde{r}_R)/\sigma_0 \end{Bmatrix} \tag{31}$$

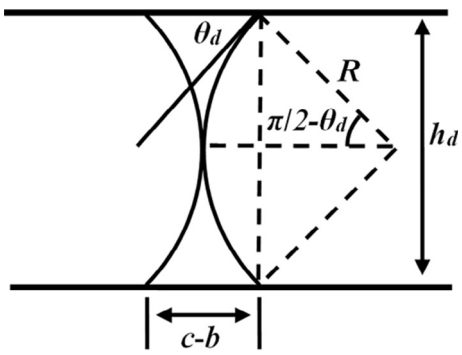

Fig. 8. The disruption of sweat bridge in equivalent crack.

$$\begin{Bmatrix} I_{11} \\ I_{12} \\ I_2 \end{Bmatrix} = \mathrm{Im}\begin{Bmatrix} \frac{\gamma\sin\theta_d}{\delta a}\left[E2(\tilde{c}) + 2E2\left(\frac{\tilde{b}+\tilde{c}}{2}\right) + E2(\tilde{b}) - E1(\tilde{c}) - 2E1\left(\frac{\tilde{b}+\tilde{c}}{2}\right) - E1(\tilde{b})\right] \\ F(\tilde{c}) + 2F\left(\frac{\tilde{b}+\tilde{c}}{2}\right) + F(\tilde{b}) \\ \frac{2\gamma\cos\theta_d}{a}\left[E2(\tilde{c}) + 2E2\left(\frac{\tilde{b}+\tilde{c}}{2}\right) + E2(\tilde{b})\right] \end{Bmatrix} \tag{32}$$

Then substituting $\tilde{h}_d$ for $\tilde{h}$ in Eq. (24) and (25) will result in the crack opening displacement and the stress intensity factors of the equivalent crack problem.

As mentioned in Fig. 6d, the crack opening displacement increases with the increase of far-field tensile stress. And it will eventually result in the disruption of the sweat bridge. By using the method of the equivalent crack, we can obtain the far-field tensile stress σ_m which can split the sweat bridge by using the following model [18].

According to the geometry of the sweat bridge in Fig. 8, we can obtain

$$\begin{cases} \frac{h_d}{2} = R\sin\left(\frac{\pi}{2} - \theta_d\right) \\ \frac{c-b}{2} = R - R\cos\left(\frac{\pi}{2} - \theta_d\right) \end{cases} \tag{33}$$

So, we can obtain the relation between h_d, $c-b$ and θ_d as

$$\frac{\tilde{h}_d}{\tilde{c}-\tilde{b}} = \frac{\cos\theta_d}{1-\sin\theta_d} \tag{34}$$

And from Eq. (27), i.e. $S = S_1 + S_2 + S_3$, the size of sweat bridge in Fig. 8 is given as

$$\tilde{S} = (\tilde{c}-\tilde{b})\tilde{h}_d - \frac{\tilde{h}_d}{2}\left(\frac{\pi/2-\theta_d}{\cos^2\theta_d} - \tan\theta_d\right) \tag{35}$$

By solving Eqs. (34) and (35), we can obtain the value of $\tilde{h}_d$ and θ_d when the wetting zone $c-b$ is given.

Then solving Eq. (29) by replacing σ_0 with σ_m, the far-field tensile stress σ_m which can split the sweat bridge is given as

$$\sigma_m = \left[4\tilde{h}_d + \frac{I_2}{\tilde{h}_d} - I_{11}\right] \Big/ I_{12} \tag{36}$$

where I_{11}, I_{12} and I_2 can be obtained by applying θ_d into Eq. (32).

Fig. 9 shows the effect of the sweat's size on the far-field tensile stress which can split the sweat bridge under different locations of sweat by using the following parameters: $a = 1\,\mu m$, $c-b = a/5$ and $\delta = 10\,nm$.

As shown in Fig. 9b, the crack closure may exist among the liquid-vapour interface although the sweat bridge is in disruption. In addition, we obtain $\tilde{h}_d$ as about 0.48 in this case. In combination with Fig. 9b, the ratio of $\tilde{h}_d$ and $\tilde{\Delta}$ is in reasonable range, so we can consider the assumption of equivalent crack is reasonable.

From Fig. 9a, when the sweat is closer to the crack tip, a larger far-field tensile stress is needed to disrupt the sweat. However, the increase of the far-field tensile stress may lead to the crack propagation and we usually do not know the exact position of sweat in practice. So, we can consider the far-field tensile stress, which can disrupt the sweat bridge, to be the criterion of the sweat's rupture in practical applications, when the sweat bridge is in the centre of the crack.

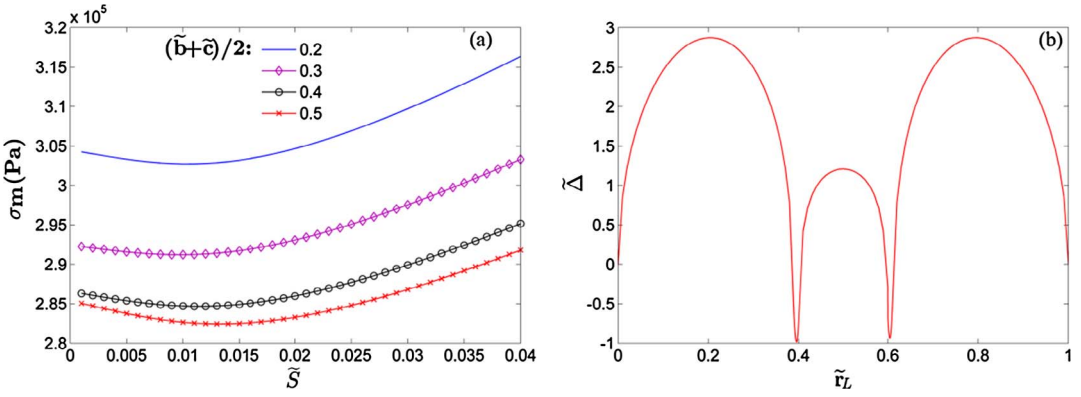

Fig. 9. (a) The far-field tensile stress, which can split the sweat bridge, under different sizes and locations of sweat bridge. (b) The crack opening when the sweat bridge is split, $\tilde{S} = 0.03$, $(\tilde{b}+\tilde{c})/2 = 0.5$.

5. Summary

To study the effect of the sweat on the interface crack between skin and flexible membrane, we regard it to be a problem of an interface crack with a liquid bridge between two crack surfaces. Considering the capillary effect of the sweat bridge, the method of Lester is used to describe the normal stress on the crack surface. The crack opening displacement and the stress intensity factors are derived by using the complex variable method. It has been found that the location of sweat plays an important role in the calculation of the stress intensity factors, although it affects the shape of crack opening slightly. With the increase of the contact angle, the crack opening displacement increases substantially. This result reveals the importance of the sweat's size on the property of the crack surface. Without or with the action of a small far-field tensile stress, the crack may be induced to partial closure. And the increase of the far-field tensile stress will increase the crack opening displacement, eventually split the sweat bridge into two parts. Due to the inconsequence caused by giving the initial thickness of sweat bridge directly in calculation, we take the assumption of equivalent crack to solve it. The far-field tensile stress causing the disruption of sweat bridge is obtained analytically. It's shown that the effect of the far-field tensile stress on disrupting the sweat bridge also depends on the sweat's size and location. In summary, the analysis reveals the importance of sweat or capillary bridge in controlling the performance and reliability of the flexible membrane.

Acknowledgements

This work is supported by the National Natural Science Foundation of China (No. 11572355, 11472313 and 11232015).

References

[1] Kim D-H, Lu N, Ma R, Kim Y-S, Kim R-H, Wang S, et al. Epidermal electronics. Science 2011;333:838–43.
[2] Lu B, Chen Y, Ou D, Chen H, Diao L, Zhang W, et al. Ultra-flexible piezoelectric devices integrated with heart to harvest the biomechanical energy. Sci Rep 2015;5:16065.
[3] Cheng H, Wang S. Mechanics of interfacial delamination in epidermal electronics systems. J Appl Mech 2013;81:044501–44503.
[4] Yung-Yu H, Hoffman J, Ghaffari R, Ives B, Pinghung W, Klinker L, et al. Epidermal electronics: skin sweat patch. In: 2012 7th international microsystems, packaging, assembly and circuits technology conference (IMPACT); 2012. p. 228–31.
[5] Wang S, Li M, Wu J, Kim D-H, Lu N, Su Y, et al. Mechanics of epidermal electronics. J Appl Mech 2012;79:031022–31026.
[6] Li K, Cai SQ. Wet adhesion between two soft layers. Soft Matter 2014;10:8202–9.
[7] Style RW, Dufresne ER. Static wetting on deformable substrates, from liquids to soft solids. Soft Matter 2012;8:7177–84.
[8] Dervaux J, Limat L. Contact lines on soft solids with uniform surface tension: analytical solutions and double transition for increasing deformability. Proc Roy Soc a – Math Phys Eng Sci 2015;471:20140813.
[9] Yu YS, Zhao YP. Elastic deformation of soft membrane with finite thickness induced by a sessile liquid droplet. J Colloid Interface Sci 2009;339:489–94.
[10] Karpitschka S, Das S, van Gorcum M, Perrin H, Andreotti B, Snoeijer JH. Droplets move over viscoelastic substrates by surfing a ridge. Nat Commun 2015;6:7891.
[11] Park SJ, Weon BM, Lee JS, Lee J, Kim J, Je JH. Visualization of asymmetric wetting ridges on soft solids with X-ray microscopy. Nat Commun 2014;5.
[12] Yang FQ, Zhao YP. The effect of a capillary bridge on the crack opening of a penny crack. Soft Matter 2016;12:1586–92.
[13] Rice JR, Sih GC. Plane problems of cracks in dissimilar media. J Appl Mech 1965;32:418–23.
[14] Sun CT, Jin ZH. Chapter 3 – the elastic stress field around a crack tip. Fracture mechanics. Boston: Academic Press; 2012. p. 25–75.
[15] Lester GR. Contact angles of liquids at deformable solid surfaces. J Colloid Sci 1961;16:315–26.
[16] Hutchinson JW, Mear ME, Rice JR. Crack paralleling an interface between dissimilar materials. J Appl Mech 1987;54:828–32.
[17] Rice JR. Elastic fracture mechanics concepts for interfacial cracks. J Appl Mech 1988;55:98–103.
[18] Meurisse MH, Querry M. Squeeze effects in a flat liquid bridge between parallel solid surfaces. J Tribol – Trans Asme 2006;128:575–84.